Laboratory measurements of the vertical structure of rip currents

Kevin A. Haas and Ib A. Svendsen
Center for Applied Coastal Research, University of Delaware, Newark, Delaware, USA

Received 11 April 2001; revised 26 July 2001; accepted 8 November 2001; published 31 May 2002.

[1] This paper describes the three-dimensional variation of rip currents through the use of experimental measurements of rip currents in a directional wave basin. The rip currents are unstable, appearing sporadically at any given location. The vertical profile of the rip current is found to vary from depth-uniform inside the channel to depth-varying further offshore. Offshore from the channel the rip current has much stronger velocities at the surface than near the bottom. The instantaneous profiles twist rapidly over depth farther offshore and are fairly uniform in the channel. The depth variations are shown to be sensitive to the total volume flux in the rip. *INDEX TERMS:* 4546 Oceanography: Physical: Nearshore processes; 4512 Oceanography: Physical: Currents; 4560 Oceanography: Physical: Surface waves and tides (1255); *KEYWORDS:* rip currents, waves, nearshore circulation, laboratory measurements

1. Introduction

[2] Since the middle of the 20th century the shores and beaches of the United States have been developing at an increasing rate. As a result of this economic buildup, it is becoming more important to understand coastal processes, consisting of wind, waves, and currents as well as the motion of the sediments, in order to better protect the shore. In the nearshore region the longshore and cross-shore currents (including rip currents) play a major role in the sediment motion. Rips also play an important role in the morphodynamical changes on a littoral beach such as the cross-shore migration of longshore bars. Extensive field observations show that rip currents form an integral part of the nearshore circulation patterns that are responsible for such changes [see, e.g., *Short*, 1979; *Wright and Short*, 1984; *Lippmann and Holman*, 1990; *Short and Brander*, 1999].

[3] Rip currents generally are created by longshore variation in the forcing. *Dalrymple* [1978] created two basic classifications of the mechanisms for creating the longshore variations necessary for generating rip currents, wave interaction models, and structural interaction models. The wave interaction models contain mechanisms such as edge waves interacting with incoming short waves, interacting wave trains, and wave-current interaction models. The structural interaction models include rips created by the bottom topography and coastal structures. The most common type of rip currents on sandy beaches in nature belongs to the latter group and occurs on barred beaches with rip channels.

[4] Rip current systems have been modeled numerically by *Noda* [1974], *Tanaka and Wada* [1984], and *Sørensen et al.* [1994], but those models were two-dimensional (2-D) horizontal models and did not include the effect of vertical varying currents. In general, however, nearshore currents vary over depth in both magnitude and direction. More recently, rip currents have been modeled by *Haas and Svendsen* [2000] and *Svendsen et al.* [2000] using the quasi 3-D numerical nearshore circulation model SHORECIRC, which accounts for the vertical variation of the currents. The validity of the vertical variation of the currents determined by the model needed to be confirmed by comparisons with measurements, and there is a lack of data in this area.

0148-0227/02/2001JC000911$09.00

[5] This lack of data is primarily because predicting where and when a rip current occurs can be difficult, thereby making measurements of rip currents in the field a challenging task. In the literature, such as by *Sonu* [1972] and *Shepard and Inman* [1950], indications are that although rip currents appear to be depth-uniform inside the surf zone, outside the breakers, rip currents tend to become surface currents. However, these indications are based on discussions with lifeguards or inferred from measurements at single locations. *Brander* [2000] measured rip velocities over depth at a single location on Palm Beach in Australia and found significant depth variations in the velocities.

[6] The vertical variation of rip currents is easier to measure in laboratory experiments. *Sasaki* [1985] measured the vertical variation of rip currents generated on a steep plane beach by the interaction between normally incident waves and the edge wave modes excited excited by the waves. These measurements, however, show little depth variation for the generated rip currents. Rip currents in a closed basin created by longshore currents encountering the side wall of the basin were measured by *Wind and Vreugdenhil* [1986]. In this situation the rip current was constrained by the side and offshore walls. The vertical profiles showed a weak depth variation with the current close to the surface only slightly larger than the current below. *Drønen et al.* [1999] conducted an experiment with only half of a rip channel and part of a longshore bar in a wave flume. The focus was on the depth variation of the flow inside the channel within the surfzone where the currents were found to be mainly depth-uniform.

[7] Previously, *Haas et al.* [1998] and *Haas and Svendsen* [2000] found that rip currents were strongly influenced by the interaction with the incoming waves. The general problems of interaction between waves and currents have been studied frequently, although the focus tends to be on the flow near the bed in the boundary layer. There have been a few experiments measuring the vertical variation of currents higher in the water column in wave flumes in the presence of waves for following and opposing (similar to a rip) currents [e.g., *Bakker and van Doorn*, 1978; *Kemp and Simons*, 1982, 1983; *Klopman*, 1994]. These experiments found that opposing currents tend to show an increase in vertical shear due to an increase in velocity near the surface. However, even in the simple 2-D case the underlying mechanism for this is largely unexplained, with only qualitative descriptions given by *Nielsen and You* [1996] and *Dingemans et al.* [1996].

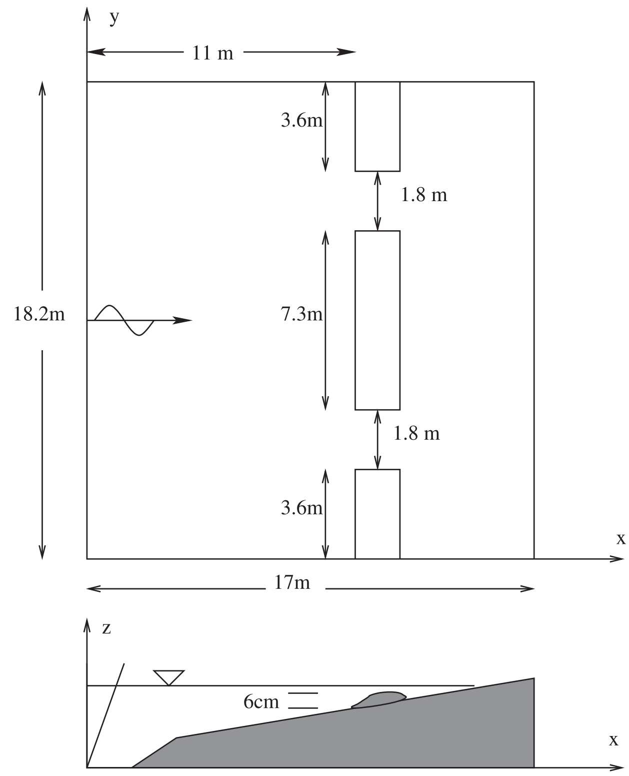

Figure 1. Design topography.

[8] The most comprehensive laboratory measurements of rip currents to date were obtained by *Haller et al.* [1997a, 1997b] and *Haller and Dalrymple* [1999]. These measurements were performed in a directional wave basin with a longshore bar and two rip channels using several different incident wave conditions. The flow velocity, wave height, and mean water level were measured over a large area, creating a detailed picture of the horizontal circulation pattern of the rip current system. However, the velocity measurements in these experiments were only taken at a single depth. This paper discusses the results from the laboratory rip currents experiments that we performed as an extension of these experiments. The goal was to investigate the vertical variation of rip currents.

[9] The difference between the measurements described here and the previous efforts is that, unlike *Sasaki* [1985], these measurements are for topographically generated rip currents. In addition, the rips measured by *Wind and Vreugdenhil* [1986] were along the side wall and were never unbounded as in the present measurements. The measurements by *Drønen et al.* [1999] were primarily in the channel, whereas our measurements extend far outside the breakers. More importantly, we have found that the assumption of symmetry around the centerline of the rip channel, which the setup of the experiment by *Drønen et al.* [1999] enforces, seriously restricts the flow and suppresses a significant part of the variations found in our experiments.

[10] This paper is organized as follows. The experimental setup is given in section 2. The experimental results are described in section 3; this includes descriptions of the temporal and depth variation of the rip currents. Section 4 is a discussion as to the significance of the findings. Finally, the conclusions are given in section 5.

2. Experimental Setup

[11] The laboratory experiment was performed in the directional wave basin located in the Ocean Engineering Laboratory at the University of Delaware. Details about the design and building of the experimental setup are given by *Haller et al.* [2000].

[12] The design of the wave basin is seen in Figure 1. The waves are created by a multipaddle wave maker located at the toe of a steep 1:5 slope preceding a milder 1:30 slope. A longshore bar of height 6 cm with two channels is centered ~11.8 m from the offshore wall, and the two channels are ~1.8 m wide.

[13] The original experiments described by *Haller and Dalrymple* [1999] focused primarily on obtaining information about a horizontal spatial overview of the rip current circulation pattern. The time-averaged wave heights and water levels $\bar{\zeta}$ from these experiments are shown in Figure 2. In Figure 2a the wave heights closest to the shoreline are facing toward the front of the figure, whereas in Figure 2b the offshore region of the water level is shown facing toward the front of the figure. The wave heights in Figure 2a are decaying at a faster rate over the bar than through the channel. This leads to a longshore pressure gradient toward the channel evident in Figure 2b. The larger waves behind the channel lead to more intense breaking closer to the shoreline, creating a pressure gradient away from the channel. The waves passing through the channel are larger than the waves passing over the bar because of the wave current interaction with the strong opposing current in the rip.

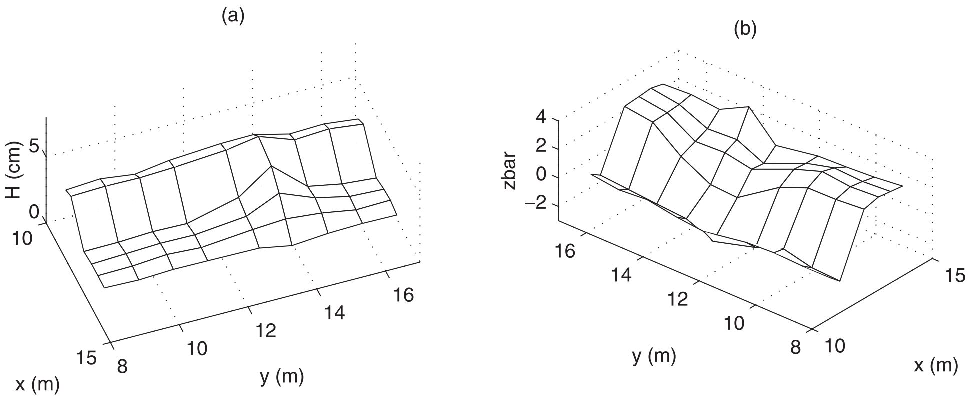

Figure 2. Mesh plots of the time-averaged (a) wave height H and (b) mean water level $\bar{\zeta}$ from *Haller et al.* [1997a]. Note that to facilitate the overview in Figure 2a, the shoreline is facing toward the front of the figure, and in Figure 2b the shoreline is facing toward the back of the figure. The rip channel is centered at y = 13.6 m.

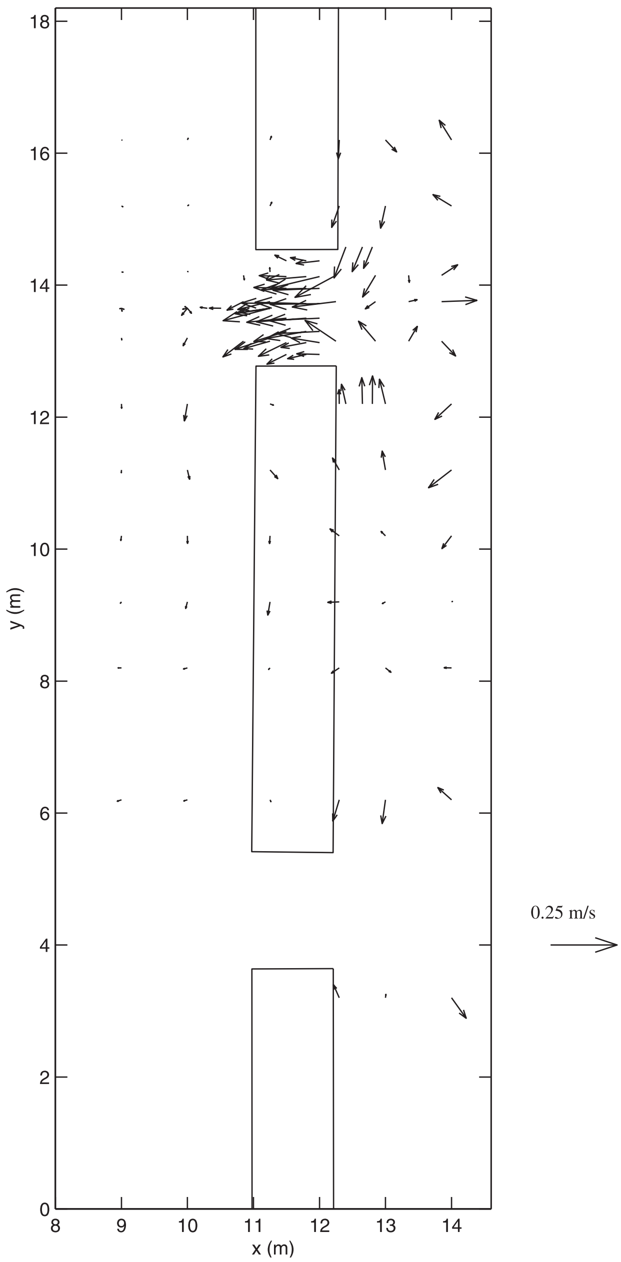

Figure 3. Time-averaged velocity vectors from *Haller et al.* [1997a, 1997b].

[14] The longer time-averaged velocity vectors from these experiments are seen in Figure 3. The measurements span a large portion of the wave basin, providing a good spatial description of the rip current system. Over and just shoreward of the bar the pressure gradient drives flow toward the rip channel. However, closer to the shoreline the pressure gradient drives flow away from the channel, generating secondary recirculation cells.

[15] It is apparent in Figure 3 that the primary focus of the measurements lies within one of the rip channels, indicated by the dense number of measurements within that channel. The rip current is biased toward the inside of the basin and appears to vanish shortly offshore of the bar. At most locations, measurements are only available for one depth that is selected at approximately mid-depth so that it gives a good representation of the depth-averaged currents.

[16] Measurements reported here are designed to supplement the experiments by *Haller and Dalrymple* [1999]. They are concentrated in the region inside and offshore of the rip channel in order to learn about the evolution of the rip as it flows offshore. The purpose of the experiments is to gain understanding of the vertical variation of the rip currents. This includes information about the temporal variation for the vertical profiles of rip currents.

[17] Three Sontek Acoustic Doppler Velocimeters (ADVs) were used for measuring the velocities. The ADVs are side-looking 2-D probes. The ADVs are mounted on a movable carriage in an arrangement indicated in Figure 4 such that they are as close to each other as possible horizontally ($\sim$7 cm). In order to measure the depth variation of the current, the probes are positioned at three different depths. The offshore gage (ADV 0) is placed near the bottom, the middle gage (ADV 1) is placed near the surface just below the trough level of the waves, and the shoreward gage (ADV 2) is placed close to mid-depth. The measurements from the three gages are used together to provide a vertical profile of the current assumed to be taken at the location of ADV 1.

[18] The water level is measured using 10 capacitance gages. The wave height as well as the mean water level (MWL) are extracted from the time series produced by these gages. All data is recorded with a frequency of 10 Hz. Details about the equipment and procedures are given by *Haas and Svendsen* [2000].

3. Experimental Results

[19] Three series of tests are presented in this paper and are divided as follows:

1. Series R was the initial test series with wave conditions matching *Haller and Dalrymple*'s [1999] test B. The purpose of the velocity measurements was to cover a broad area in and offshore of the rip channel and to provide an overview of the vertical variation of the rip.
2. Series S had the same wave conditions as series R. More detailed velocity measurements were taken along the centerline of the channel. Only enough wave measurements to verify repeatability were taken.
3. Series T had larger waves and does not specifically match any tests from *Haller and Dalrymple* [1999]. Therefore a wide range of wave measurements was performed to get a broad view of the wave field. The velocity measurements were along the centerline of the rip channel.

[20] The gage locations for the three test series are shown in Figure 5. Notice that we use a different coordinate system than *Haller and Dalrymple* [1999]. Each cross represents the location of the ADV array composed of three separate ADVs. The circles in Figure 5 represent individual wave gages. One wave gage is always located offshore (x = 6 m, y = 16.2 m) and is used to check repeatability of the experiments. In order to provide water level data close to the current measurements, another wave gage is always placed close to the ADV array. The remaining wave gages are placed on a bridge spanning the longshore direction.

[21] The repeatability of the experiments is summarized in Table 1, which shows the mean wave heights H_m and standard deviation σ_H for the measurements at the offshore wave gage. The test series all have variations below 3%, whence we believe the experiments are repeatable.

[22] As mentioned, test series R and S are designed to match series B from *Haller and Dalrymple* [1999]. Series B has an offshore mean wave height of 4.11 cm. Table 1 indicates that the percent deviation between the present tests and *Haller and Dalrymple* [1999] is low. Therefore we feel that we are reproducing the results from test B.

3.1. Test R: Initial Test Series

3.1.1. Temporal variations of the flow. [23] To facilitate the analysis, the time series are low-pass filtered to remove the

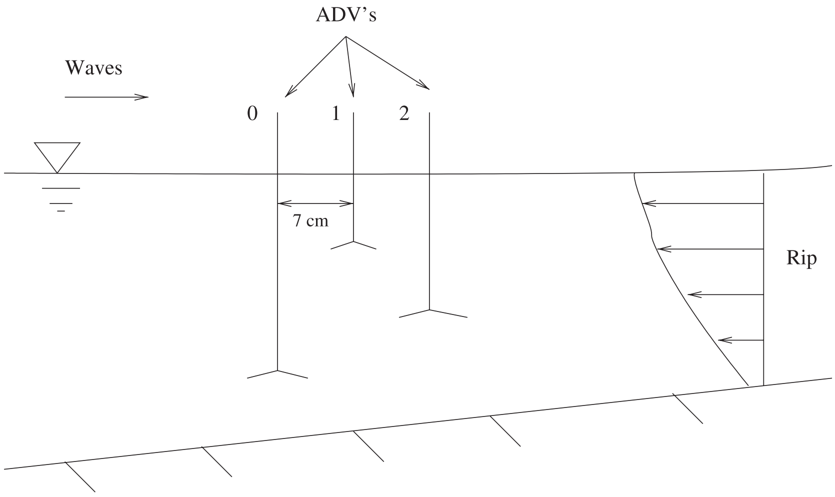

Figure 4. Setup for the ADVs.

signal from the short waves. The low-pass filter is accomplished by Fourier transforming the time series, setting the coefficients for frequencies above 0.03 Hz to zero, and inverse transforming back to the time domain.

[24] Figure 6 shows the low-pass filtered cross-shore velocity time series, measured close to the water surface for three different cross-shore positions along the centerline of the channel. In addition, a line indicating the mean value of the current, averaged

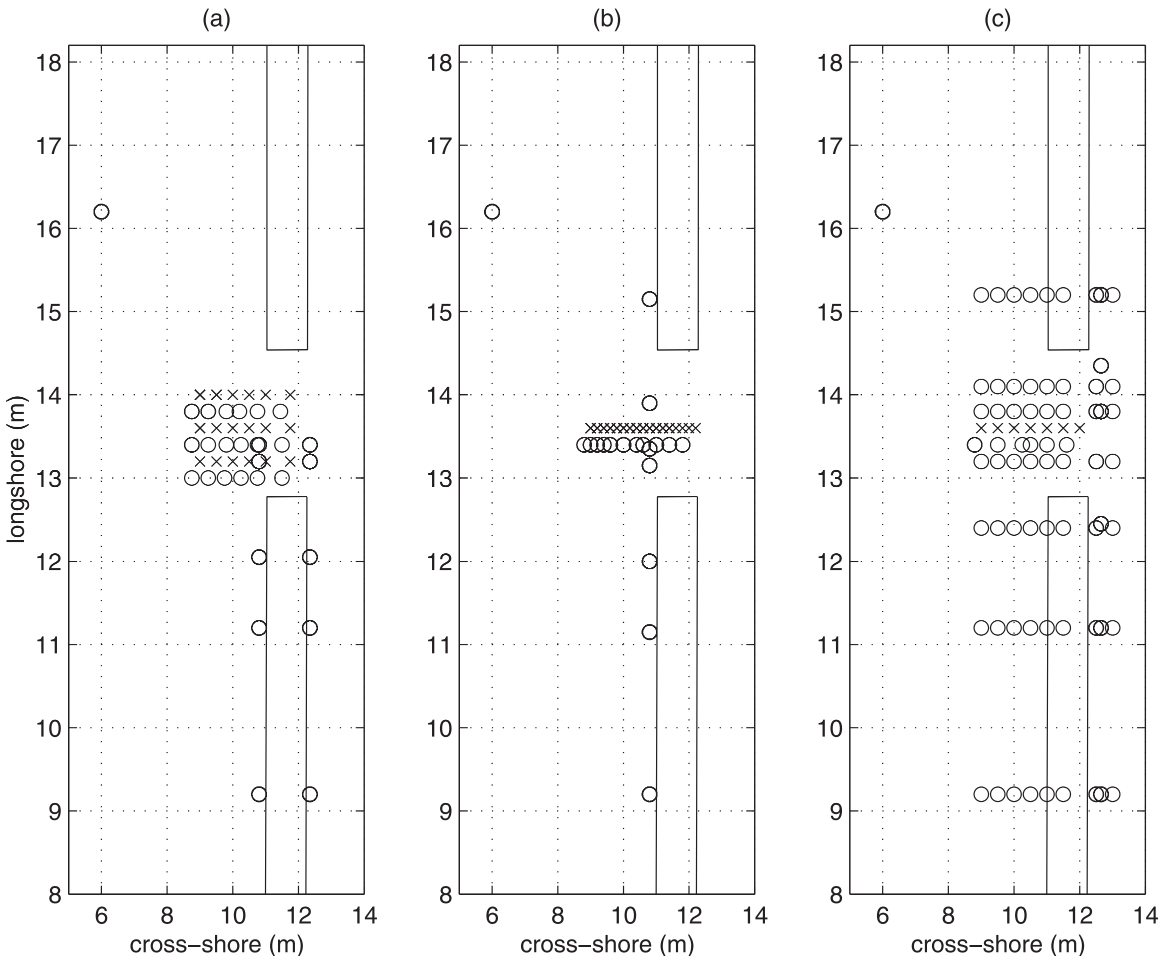

Figure 5. Location of the gages for (a) test R, (b) test S, and (c) test T. Crosses indicate ADV gage array locations, and circles indicate wave gage locations.

Table 1. Repeatability of Experiments Based on Wave Measurements at the Offshore Gage

n[a]	Test	Wave Period, s	H_m[b], cm	σ_H[c], cm	Variation, %	Deviation From Test B[d], %
18	R	1	4.04	0.08	2.0	1.7
30	S	1	4.06	0.07	1.7	1.2
16	T	1	5.79	0.12	2.1	NA[d]

[a] Number of Realizations.
[b] Offshore mean wave height.
[c] Standard deviation.
[d] NA, not applicable.

over the entire time series, is drawn on each plot (negative velocity indicates an offshore flow). These plots demonstrate that the flow in the rip varies significantly with time.

[25] At the position farthest offshore (x = 9 m; Figure 6a), the rip only occurs sporadically. Therefore the mean value of the velocity when averaged over the entire time period is small. The mean velocity is ~2 cm/s, whereas the peak velocity in the rip reaches as high as 12 cm/s. This helps to explain why the time-averaged rip in Figure 3 appears to vanish offshore. The time series in Figure 6b from the position at x = 10.5 m continues to show sporadic rip events, although more frequently than in Figure 6a. Again, the mean velocity is small, reaching a value of 4 cm/s with the peak velocity being much larger, around 20 cm/s. Only the time series in the channel (x = 11.75 m; Figure 6c) has a mean velocity that is representative of the rip. The mean value is ~17 cm/s, while the peak velocity is ~25 cm/s.

[26] Thus it appears that at any given location the rip only occurs sporadically, especially farther offshore. Even inside the channel the rip is not always present; around 100, 900 and 1500 s in Figure 6c, the rip velocity has almost vanished. When the rip velocity decreases in a time series, it does not necessarily mean that the rip has vanished all together. The rip is also moving from side to side even within the channel; therefore, as the rip moves past a gage, it shows up as a burst in the velocity. Visual observations during the experiments help confirm what happens to the rip. By watching the changes in the wave pattern, the location of the rip is identified. The rip causes the waves to refract toward the current from both sides. In addition, the wave height is increased due to the wave current interaction. We are able to watch the rip move from side to side within and offshore of the channel. There are times when the rip moves out of the channel and over the bar or even vanishes all together.

3.1.2. Depth variations of the flow. [27] Velocity measurements were taken at three depths for all locations, and time series for all three depths are examined. Figure 7 shows the cross-shore and longshore low-pass filtered velocities for all three depths measured at the centerline of the channel, offshore of the bar at x = 9 m. In Figure 7, strong depth variations clearly exist in the cross-shore velocity. For example, around t = 950 s, there is a strong rip occurrence. The cross-shore velocity closest to the surface is large, ~12 cm/s, but at mid-depth the cross-shore velocity is smaller, only around 4 cm/s. Yet, close to the bottom, the cross-shore velocity is ~2 cm/s and is even directed shoreward. The trend of shoreward velocity at the bottom continues throughout most of the time series, with only a few exceptions of offshore flow. Throughout this time series at the offshore location the cross-shore velocity in the rip rarely penetrates to the bottom of the water column. However, the longshore velocity in Figure 7b demonstrates fairly depth-uniform behavior.

[28] Similarly, Figure 8 shows the low-pass filtered velocities inside the surfzone in the middle of the channel at x = 11.75 m. Here the cross-shore velocities are almost uniform in depth. More depth variation occurs in the longshore flow shown in Figure 8b

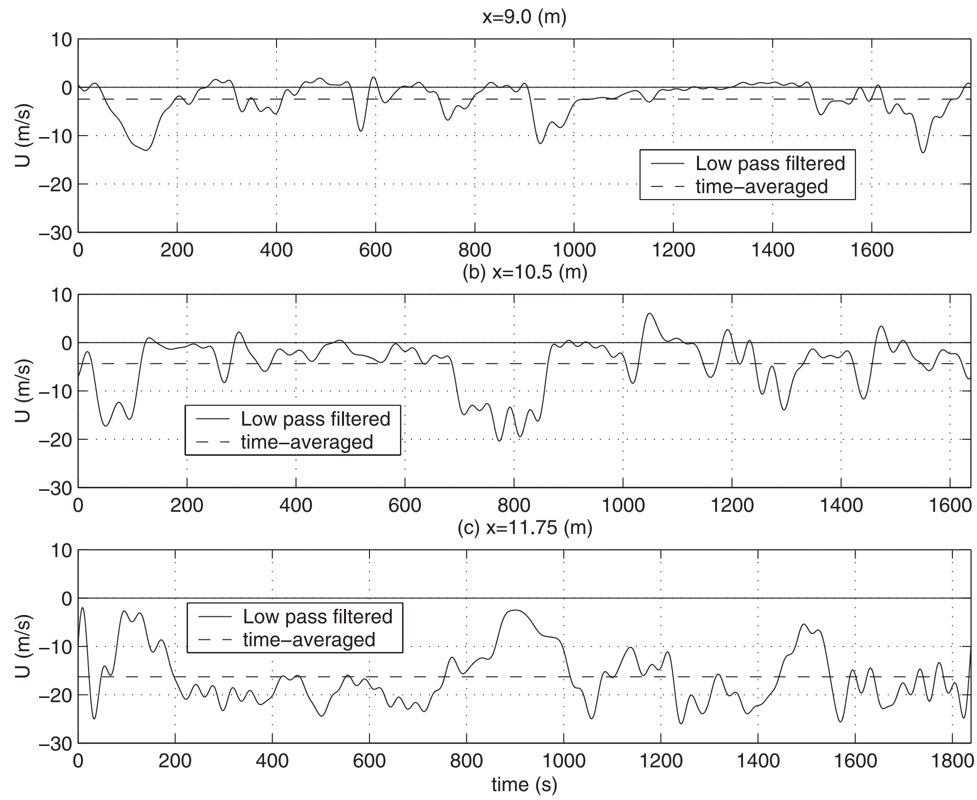

Figure 6. Low-pass filtered velocity time series from near the surface with the long-term time average along the centerline of the channel. (top) Run R17 (x = 9 m). (middle) Run R6 (x = 10.5 m). (bottom) Run R8 (x = 11.75 m).

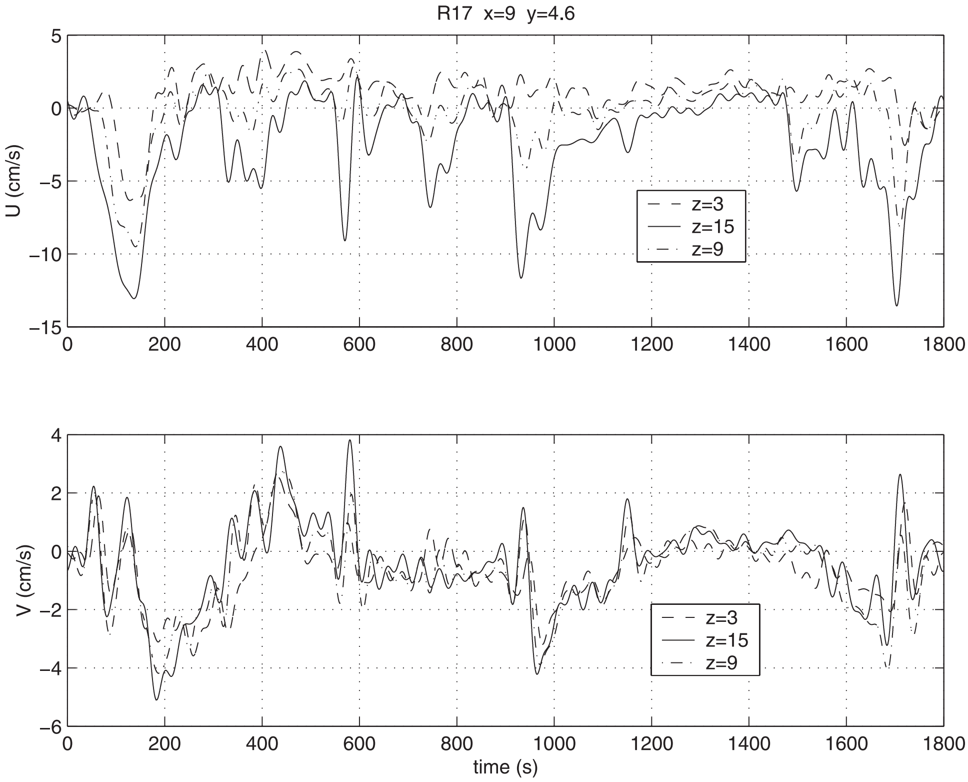

Figure 7. Low-pass filtered velocity time series at three depths 2 m offshore of the rip channel (R17, x = 9 m). The top shows cross-shore velocities (U), and the bottom shows longshore velocities (V). The value of z is 0 at the bottom and is positive upward, measured in centimeters.

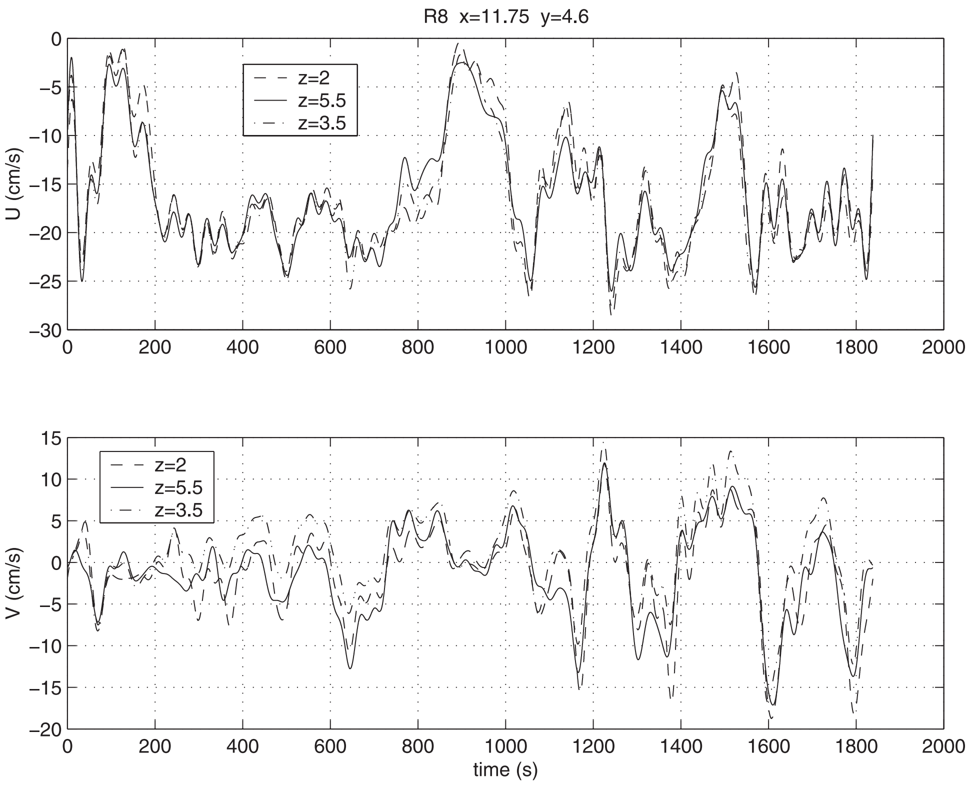

Figure 8. Low-pass filtered velocity time series at three depths in the center of the rip channel (R8, x = 11.75 m). The top shows cross-shore velocities (U), and the bottom shows longshore velocities (V). The value of z is 0 at the bottom and is positive upward, measured in centimeters.

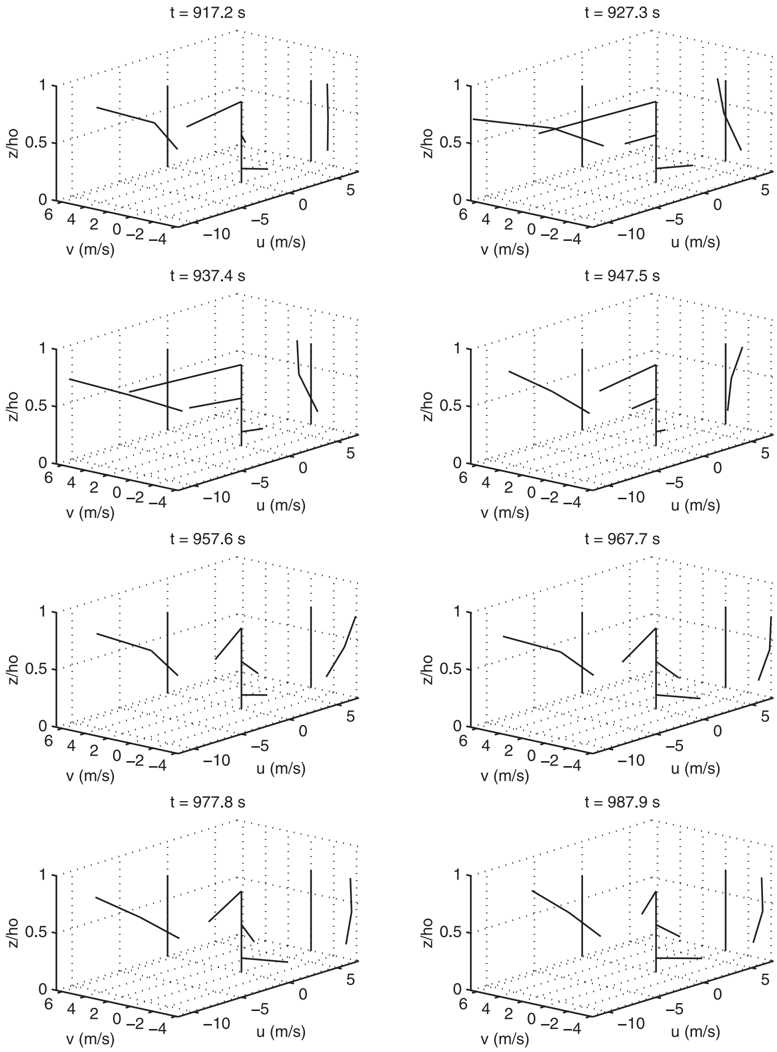

Figure 9. Snapshots of the velocity vectors with projections of the cross-shore and longshore currents for run R17 2 m offshore of the channel (x = 9, y = 13.6 m).

than in the cross-shore flow in Figure 8a. In addition, the magnitude of the longshore current is similar to the magnitude of the cross-shore current.

[29] The depth variations also give another reason why the rip current in Figure 3 vanishes shortly offshore of the channel for the time-averaged velocities. Most of the measurements used to generate the velocity vectors in Figure 3 were taken at mid-depth or lower. As seen in Figure 7, measurements at mid-depth or lower offshore of the channel have much lower velocities than the measurements taken close to the surface. This leads to the possibility that the rip does not vanish as it flows offshore. Rather, it passes over the top of the gages located lower in the water column. It should be noted that the focus of the study by *Haller and Dalrymple* [1999] is on the rip velocities in the channel, where, as indicated in Figure 8, the velocities are nearly uniform over depth so that measurements lower in the water column are representative of the velocity over all depths.

[30] At any given location, variations of the velocity profiles in time can be examined. Because the gages are offset by 7 cm in the cross-shore direction, the measurements contain some phase shift between the different depths. For this reason, instantaneous profiles are calculated by averaging the velocity over 5 s, which is usually much greater than the time it takes the flow to pass from one gage to the other. However, this timescale is much shorter than the time variations of the rip flow; therefore, little information is lost from the averaging process.

[31] Vertical profiles of velocity from eight closely spaced times during a rip event at the location 2 m offshore of the bar (x = 9 m, y = 13.6 m) are shown in Figure 9. The vertical lines are the reference lines. The lines parallel to the U and V axes are vectors indicating both the magnitude and direction of the current. The projections of the cross-shore and longshore velocities on the (U, Z) and (V, Z) faces of the display are also shown. The largest offshore (negative) current is located at the top, whereas the weakest or onshore (positive) current is at the bottom. The cross-shore velocities exhibit the strong depth variations, but the longshore velocity remains fairly depth-uniform. The striking features are that the current is twisting over depth, with the surface velocity going mainly offshore and the bottom current going in the negative longshore direction and slightly shoreward. However, at this location (x = 9 m), both magnitudes and the directions of the velocities in a profile change relatively rapidly with time.

[32] In contrast, Figure 10 shows vertical profiles of velocity at eight times during a rip event inside the channel. Here the vertical profiles tend to be depth-uniform with little twisting of the current evident. During the initial surge of the rip the peak

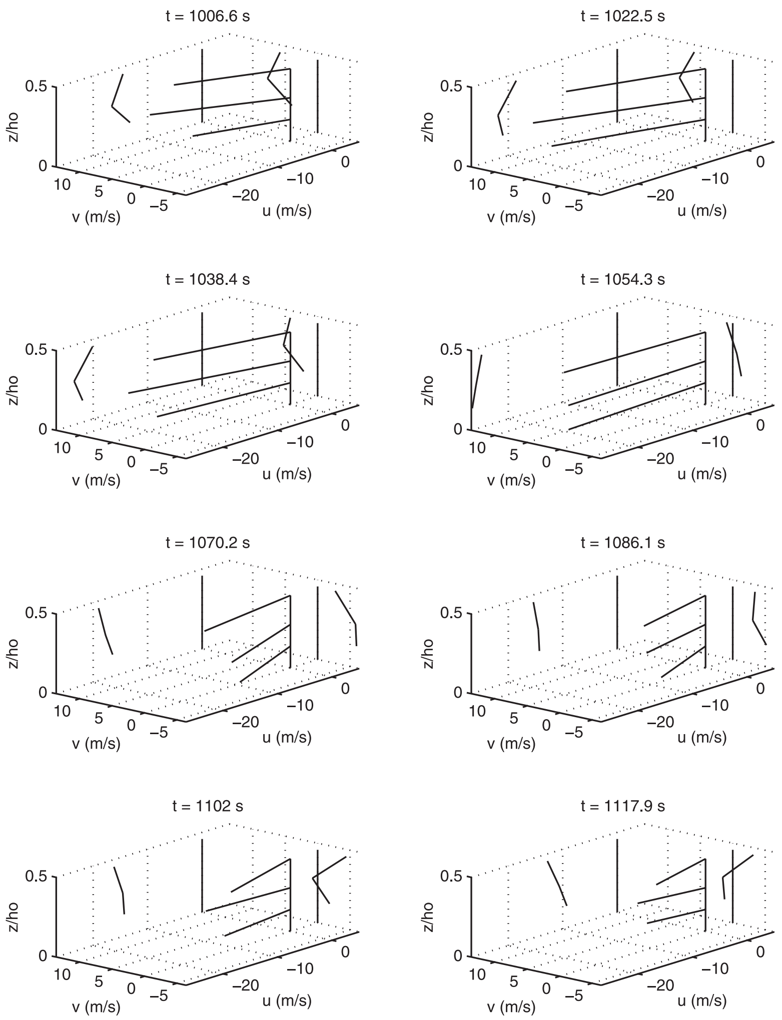

Figure 10. Snapshots of the velocity vectors with projections of the cross-shore and longshore currents for run R8 in the channel (x = 11.75, y = 13.6 m).

current is occurring at mid-depth, although as the velocity reduces, the peak tends to move toward the surface.

3.1.3. Cross-shore variations of the flow. [33] At each horizontal location the velocities are measured during separate runs, which prevents direct comparisons between the time series because the temporal variations of the rip is not identical between runs, that is, even measurements at the same location for separate runs show different temporal variations. The repeatable aspect of the experiments is the time-averaged properties and not the instantaneous flow patterns. However, as previously mentioned, time averaging the velocity records over the length of the experiments virtually eliminates the rip signal outside the surfzone.

[34] Therefore, in order to analyze the cross-shore variation of the rip current profiles, a bin-averaging technique is utilized. The velocity profiles are sorted into bins on the basis of the magnitude of the cross-shore velocity measured closest to the surface (U_1). The bins are defined using the following criteria:

$$U_1 > 25 \quad \text{bin 25}$$

$$25 > U_1 > 20 \quad \text{bin 20}$$

$$20 > U_1 > 15 \quad \text{bin 15}$$

$$15 > U_1 > 10 \quad \text{bin 10}$$

[35] The velocity profiles are averaged within each bin, producing four velocity profiles, one for each bin. The bin averaging is performed at each measurement location, and that allows for direct comparisons between the velocity profiles at different locations. The intention is to group the profiles on the basis of physical similarities.

[36] Figure 11 shows the velocity profiles for each bin at all of the locations. Since there are three measuring sites in the longshore direction for each cross-shore location, there are measurements of three profiles at each cross. The cross-shore velocity near the surface does not meet the criteria for the bins at all of the locations, which explains the absence of many profiles, especially for bin 25 in Figure 11a. The three profiles at any given cross-shore location show little variation, implying that regardless of where the rip passes in the longshore direction, the vertical profile of the cross-shore flow in the rip remains unchanged. Thus measurements at different longshore locations within the region where the rip passes produce the same velocity profile whenever the rip is present; therefore test series S and T focused primarily on one cross-shore section along the centerline of the channel.

[37] The cross-shore transition of the depth variation is evident, particularly in bin 10. Inside the channel the velocity is virtually depth-uniform, whereas the velocity exhibits strong depth variations farther offshore. It is emphasized that the profiles represent the bin-averaged velocities and are not an indication of the instantaneous depth variations. Therefore the profiles in

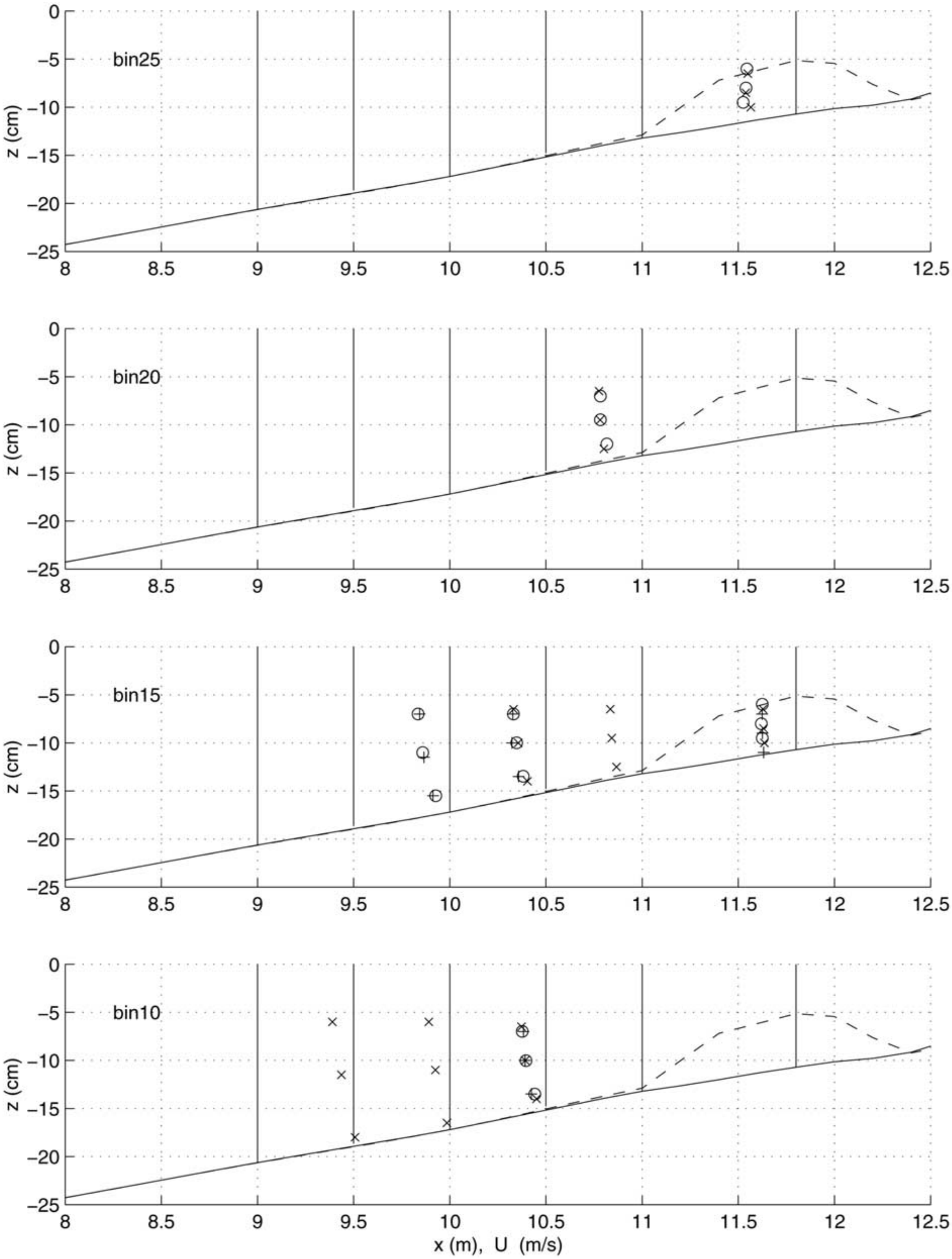

Figure 11. Bin-averaged offshore velocity profiles along three cross-shore lines from test R for (a) bin 25, (b) bin 20, (c) bin 15, and (d) bin 10. The symbols are defined as follows: crosses, $-y$ = 13.2, circles, $-y$ = 13.6, and pluses, $-y$ = 14.0. The vertical lines are the reference lines for each location.

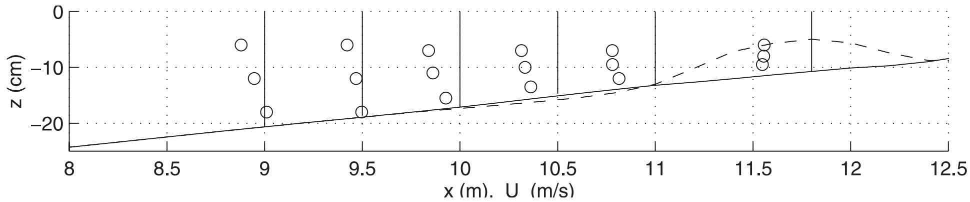

Figure 12. Maximum averaged offshore velocity profiles for test R.

Figure 11 do not represent the actual instantaneous depth variation of a rip current flowing offshore.

[38] Another technique that gives more physical representations of the cross-shore variation of the vertical current profiles is to average the maximum profile at each location. Any profile that is within 3 cm/s of the maximum velocity at the surface for a given cross-shore location is grouped together and averaged. This is based on the premise that the maximum averaged profile represents the decrease in velocity as the rip flows seaward into deeper water.

[39] Figure 12 shows the maximum averaged current profiles from test R. The peak velocity decreases as the rip flows offshore. Again, the variation of the vertical profile is evident, and there is little variation inside the channel and progressively larger depth variation farther offshore. For the location furthest offshore (x = 9 m) the velocity at the bottom even becomes shoreward.

[40] Thus the results of test R can be summarized as follows:

1. The rip currents are unstable, appearing sporadically at a given location.

2. Rip currents show a strong depth variation outside the breakers and little depth variation inside the channel.

3. The instantaneous profiles twist rapidly over depth farther offshore, while they are fairly uniform in the channel.

4. Bin averaging and maximum averaging provide good spatial descriptions of the cross-shore profiles.

3.2. Test S: Higher Resolution Test Series

[41] Because the bin-averaged rip current profiles remain the same along the three cross-shore sections in test R, a series of experiments were conducted where the focus was along a single cross-shore section. In order to get better resolution of the vertical current profiles, 13 of the locations have 6 measurements over depth from 2 separate runs. Gage 1 was kept close to the same depth near the surface to allow for direct comparison between the two runs. This yields velocity measurements at five depths for each of these locations.

[42] Low-pass filtered time series of the cross-shore and longshore velocities are shown in Figures 13 and 14. These figures are for two individual runs with the gages located at the same cross-shore and longshore positions (x = 9 m, y = 13.6 m), but the gages are at different depths. However, the gage closest to

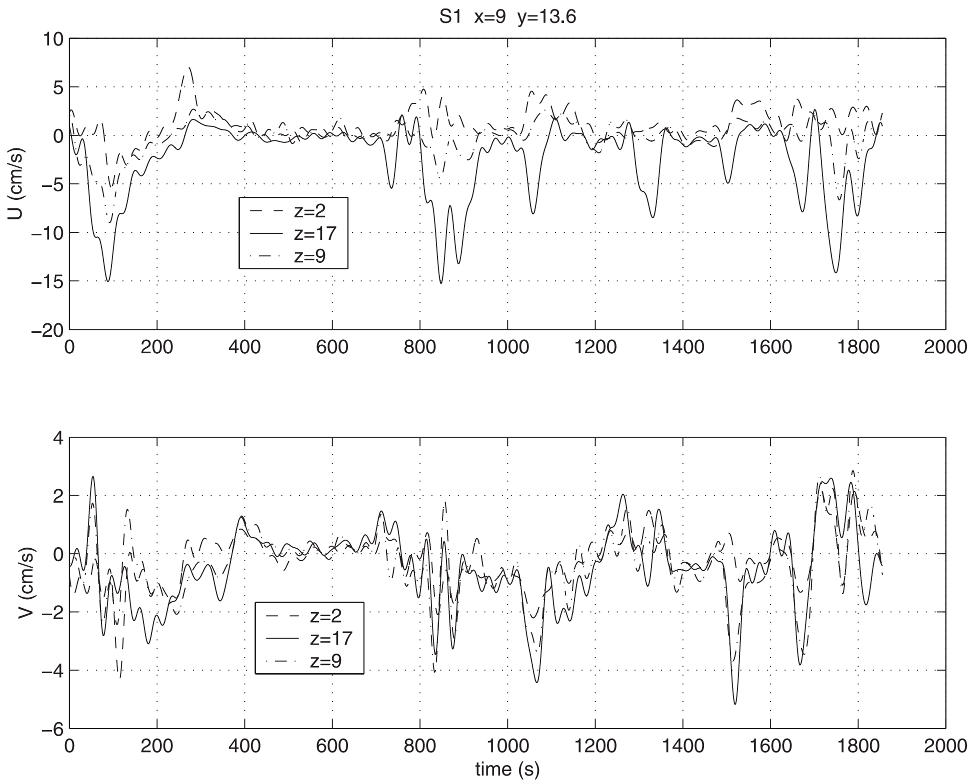

Figure 13. Low-pass filtered velocity time series at three depths 2 m offshore of the channel (S1, x = 9.0 m). The top shows cross-shore velocities (U), and the bottom shows longshore velocities (V). The value of z is 0 at the bottom and is positive upward, measured in centimeters.

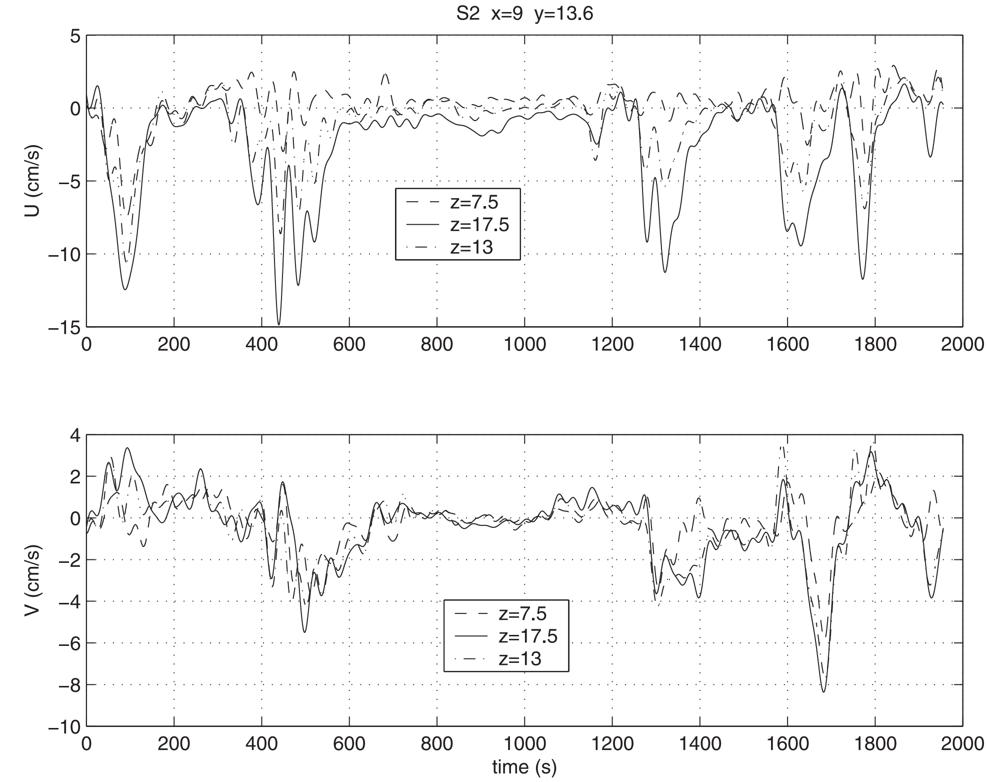

Figure 14. Low-pass filtered velocity time series at three depths 2 m offshore of the channel (S2, x = 9.0 m). The top shows cross-shore velocities (U), and the bottom shows longshore velocities (V). The value of z is 0 at the bottom and is positive upward, measured in centimeters.

the surface is at the same depth for both realizations, which allows for a direct comparison. The still water depth at this location, 2 m offshore from the bar along on centerline of the channel, is 21.0 cm.

[43] The strong depth variations are evident in Figures 13 and 14, particularly during the periods where strong rip flows are present. The velocity at the surface gage reaches up to 15 cm/s, while the velocity lower in the water column is much smaller. The cross-shore velocity closest to the bottom, plotted in red in Figure 13, is virtually always shoreward. Only the gages closest to the surface in Figures 13 and 14 and the mid-depth gage in Figure 14 record velocities which exceed 5 cm/s during the rip events. This further clarifies the impression obtained from the bin-averaged profiles that the larger currents in the rip penetrate less than half of the water column at this offshore location.

[44] We also notice that even though the wave conditions for the two experimental runs are identical, comparing the time series for the gage closest to the surface in both figures shows that the individual rip events differ. A comparison between Figures 7, 13, and 14 illustrates the remarkable variability in the temporal development of otherwise identical repetitions of the experiment. All of the time series have an initial event near the beginning, which is due to the drainage from the initial surge of water shoreward when the waves are begun. The time series in Figure 13 does not have another significant rip event until t = ~800 s, while the time series in Figure 14 has a rip event before t = 400 s. Because rip events at the same location do not occur at the same time in separate runs, direct comparisons of the time varying currents are not possible.

[45] Figures 15 and 16 show time series of the low-pass filtered velocity 1 m offshore of the bar at the centerline of the channel. The surface measurements are taken at the same depth while the other four measurements are taken at different depths, two for each figure. The still water depth at this location is 17.5 cm.

[46] At this location the rip events are sporadic and the velocities are largest close to the surface. It is interesting to note that in Figure 15, there are frequent small rip events with only a few large events with short durations. However, in Figure 16, there are a few large rip events with longer durations and almost no small rip events. Even though the measurements are taken at the same location under the same wave conditions, the rip behavior has remarkable variations.

[47] Similarly, time series of the low-pass filtered velocity measured inside the channel at x = 11.4 m are shown in Figures 17 and 18. The velocities from the gage closest to the surface are measured at the same depths, while the other gages are at four different depths. The still water depth at this location is 12.25 cm.

[48] During rip events in Figures 17 and 18 the velocities are similar at all depths. This indicates nearly depth-uniform flow for the rip inside the channel. The velocities during the lulls between rip events, however, demonstrate some depth variation with the velocity closest to the bottom being weaker or even shoreward. The frequency of rip events is similar in both figures, although in Figure 17 there is a long stretch without any rip activity for $600 < t < 800$ s. There is no such lull in rip activity in Figure 18.

[49] The velocities are separated into bins following the method outlined in section 3.1. At the cross-shore locations where two individual runs are performed, the gage closest to the surface is at the same depth for both runs. This is the velocity record that is used to sort the velocity profiles into the bins. Because the sorting is based on velocities at the same depth, the profiles from both runs are combined to give a resulting profile with velocities at five depths.

[50] Figure 19 shows the resulting vertical profiles of the cross-shore velocity for the four bins. In bin 20 the current profile shows strong depth variation at x = 10 m but weak

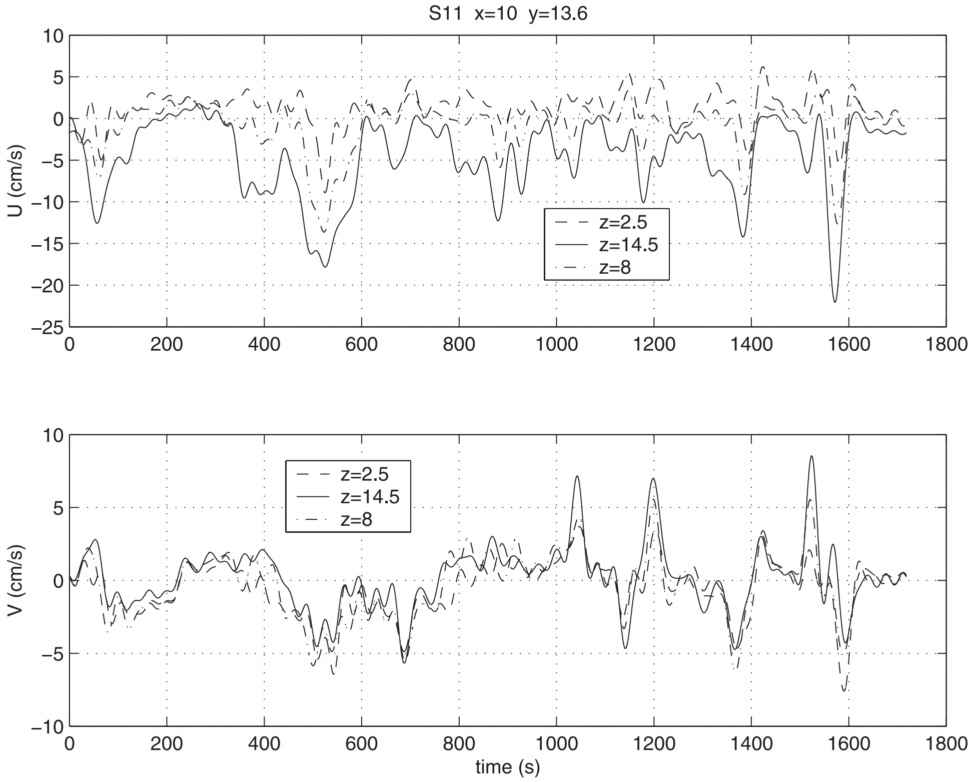

Figure 15. Low-pass filtered velocity time series at three depths 1 m offshore of the channel (S11, x = 10.0 m). The top shows cross-shore velocities (U), and the bottom shows longshore velocities (V). The value of z is 0 at the bottom and is positive upward, and measured in centimeters.

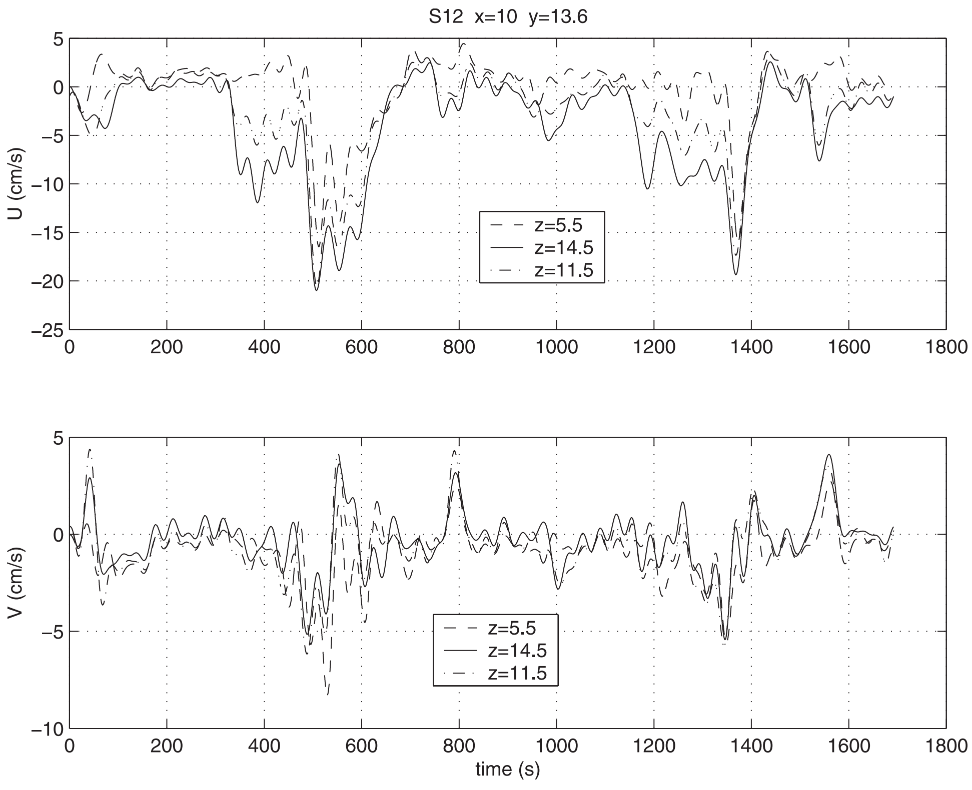

Figure 16. Low-pass filtered velocity time series at three depths 1 m offshore of the channel (S12 x = 10.0 m). The top shows cross-shore velocities (U), and the bottom shows longshore velocities (V). The value of z is 0 at the bottom and is positive upward, measured in centimeters.

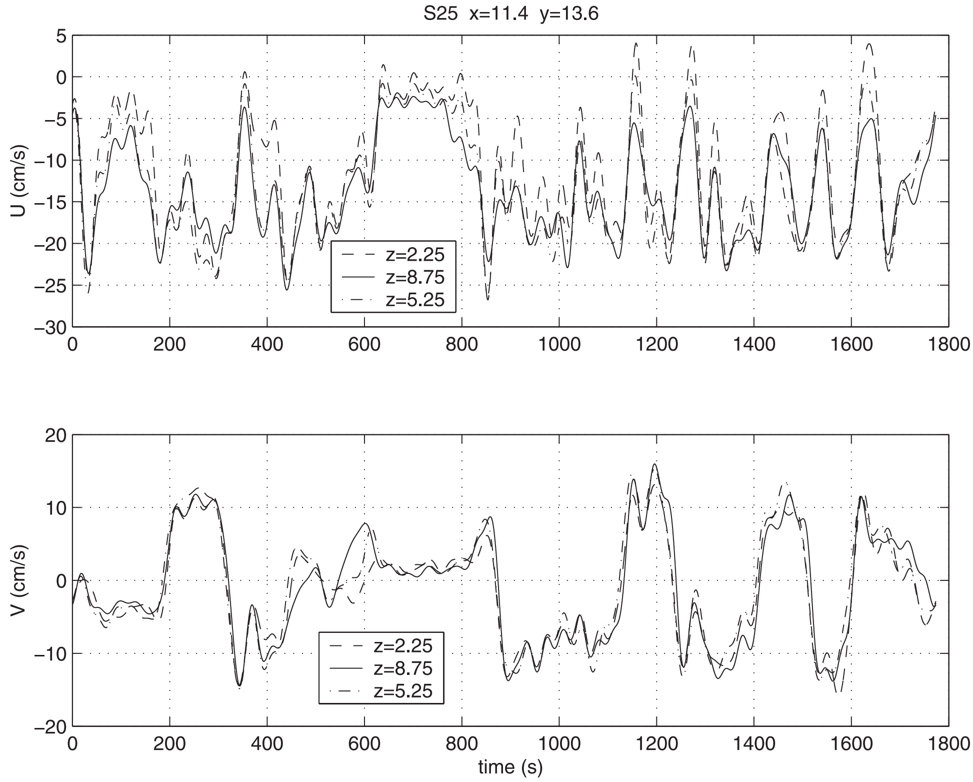

Figure 17. Low-pass filtered velocity time series at three depths inside the channel (S25, x = 11.4 m). The top shows cross-shore velocities (U), and the bottom shows longshore velocities (V). The value of z is 0 at the bottom and is positive upward, measured in centimeters.

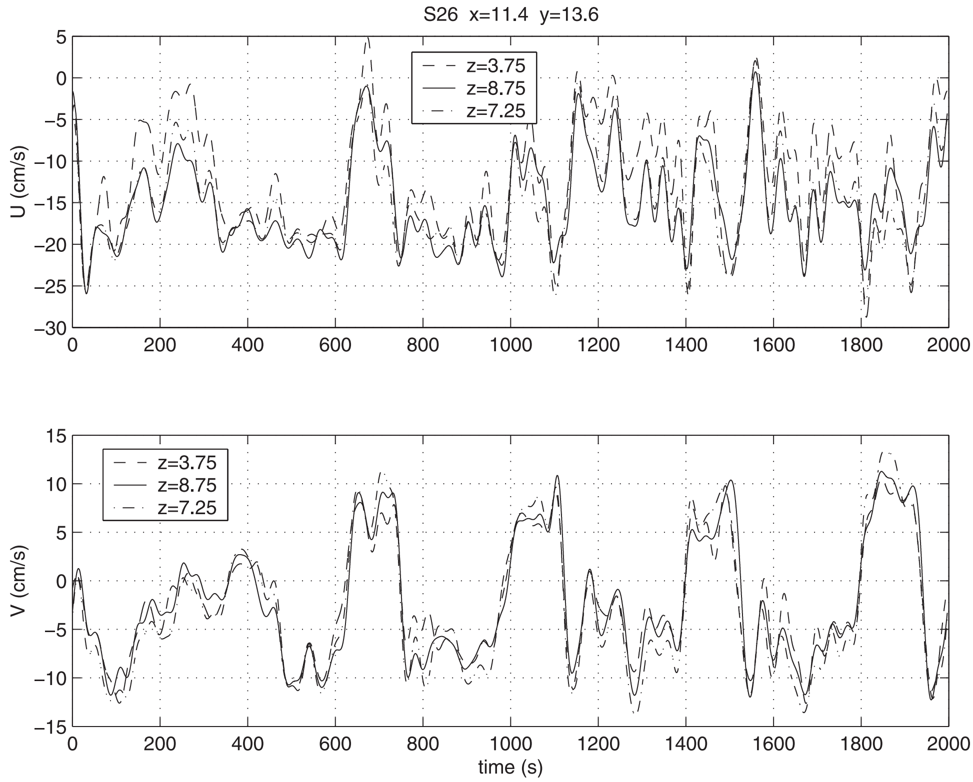

Figure 18. Low-pass filtered velocity time series at three depths inside the channel (S26, x = 11.4 m). The top shows cross-shore velocities (U), and the bottom shows longshore velocities (V). The value of z is 0 at the bottom and is positive upward, measured in centimeters.

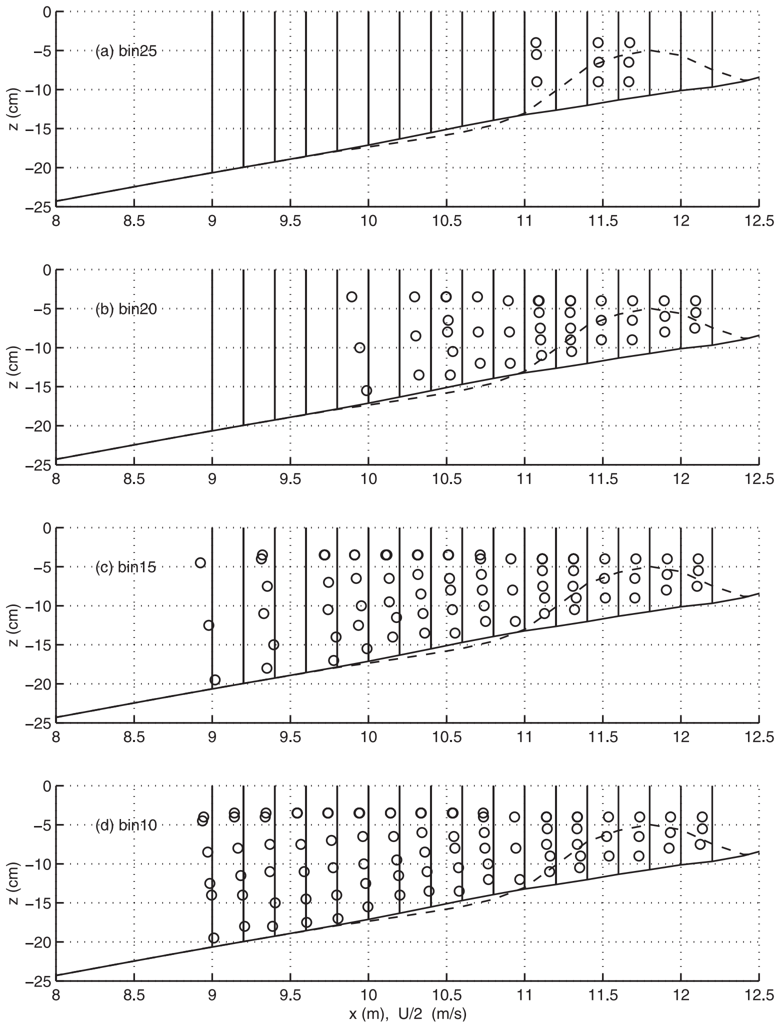

Figure 19. Bin-averaged rip current profiles from test S for (a) bin 25, (b) bin 20, (c) bin 15, and (d) bin 10. The vertical lines are the reference lines for each location.

variations for $x > 11.6$ m. The profiles in bin 10, however, show depth variations from $x = 9$ m all the way to $x = 11$ m. This indicates that stronger burst of rip flow remain depth-uniform farther offshore of the channel, but eventually all rips become surface currents. This demonstrates that the vertical profile is somewhat dependent on the total volume flux of the rip flow.

[51] At most locations, combining the separate runs to create a single profile appears to be acceptable, with only a few strange-looking profiles. Most importantly, the bin-averaged velocity for the surface measurements show good agreement even though they are from different runs. Although the time series of rip events for separate runs at the same location have varying frequency and duration of rip events, the bin-averaged velocity at the surface remains unchanged.

[52] In summary, test series S showed that even at the same location the rip events were different for separate runs. This series also provides much more detailed vertical profiles. It is found that the larger rip bursts containing more volume flux has less depth variation than smaller rip bursts at the same location.

3.3. Test T: Large Wave Test Series

[53] This test represents a situation characterized by larger waves. The larger waves carry more water over the bar, leading to greater offshore discharge in the rip currents. Because the depth is the same as for the smaller wave case, the larger discharge leads directly to larger velocities in the rip current. The purpose of this test is to analyze the sensitivity of the vertical profiles to increased total flux in the rip current.

[54] For this test we have extensive wave and mean water level records (see Figure 5c). The time-averaged wave heights and water levels $\overline{\zeta}$ from test T are shown in Figure 20a. In Figure 20a the wave heights closest to the shoreline are facing toward the front of the figure, whereas in Figure 20b the offshore region of the water level is shown facing toward the front of the figure. The increase of wave height due to the presence of the rip current is evident around $y = 13.6$ m. The decrease in the wave height as the waves break over the bar ($x = 12$ m) is seen as well. The water level in Figure 20b shows a setdown offshore of the breaking followed by setup closer to the shoreline. In the trough region behind the bar ($x > 12$ m) the setup is larger behind the bar ($y < 13$ m) than behind the channel ($y = 13.6$ m), leading to a longshore pressure gradient toward the channel.

[55] A more detailed view of the cross-shore variation of the time-averaged wave heights and water levels is shown in Figure 21. As the waves approach the offshore edge of the bar ($x = 11$ m), the wave height in the channel is increasing rapidly, whereas the wave height over the bar is actually decreasing slightly. The exact location of the breaking is difficult to identify because of the coarse resolution of the measurements. The waves that passed over the bar seem to have stopped breaking and to be

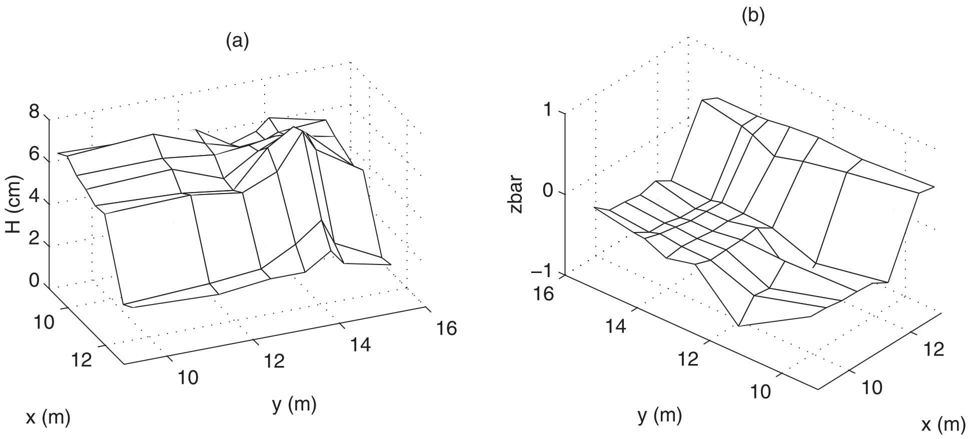

Figure 20. Mesh plots of the time-averaged (a) wave height H and (b) mean water level $\bar{\zeta}$ for test series T. Note that to facilitate the overview in Figure 20a, the shoreline is facing toward the front of the figure and in Figure 20b the shoreline is facing toward the back of the figure. The rip channel is centered at y = 13.6 m.

reforming and increase slightly in height for $x > 12.5$ m. The waves passing through the channel, however, are decreasing in height between $x = 12.5$ and $x = 13$ m, indicating that the waves are still breaking.

[56] The equivalent cross-shore sections of the mean water level over the bar and channel are shown in Figure 21b. Offshore from the bar ($x < 11$ m), there is little longshore difference in the setdown. Once breaking commences and a setup is created, the longshore decrease of $\bar{\zeta}$ toward the channel in the trough behind the bar for $x \geq 12.5$ m becomes evident, as indicated in Figure 20. For $x \geq 12.5$ m the setup behind the bar is significantly larger than the setup behind the channel. At the shoreward most point, $x = 12$ m, the difference between the water levels is smaller, suggesting that further measurements even closer to the shoreline would show a reversal of the longshore pressure gradient.

[57] Time series of the low-pass filtered velocity for three depths measured 2 m offshore of the channel ($x = 9$ m) are shown in Figure 22. Comparing this figure with Figure 7 reveals that for the larger wave conditions the rip occurs much more frequently and has stronger velocities. Figure 22 also shows that the cross-shore velocity measured by the bottom gage is usually shoreward, although for a few strong bursts the velocity is seaward. Similar to the weaker wave conditions, the longshore current shows less depth variation than the cross-shore current.

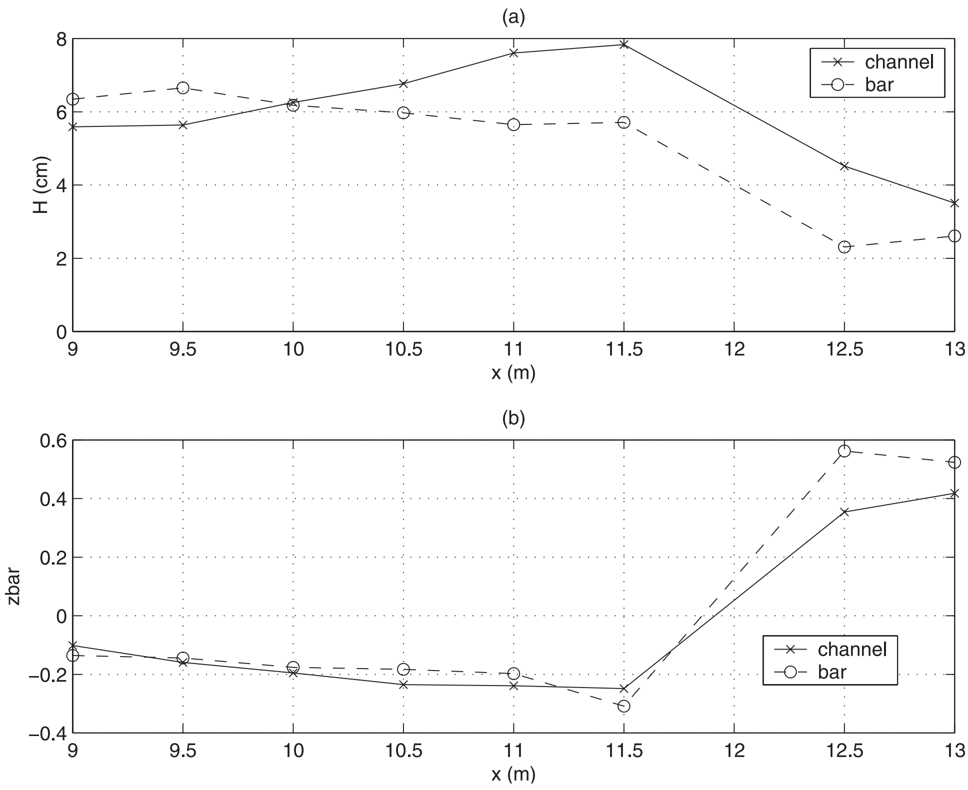

Figure 21. Cross-shore sections of the time-averaged (a) wave height H and (b) the mean water level $\bar{\zeta}$ through the channel (y = 13.5 m) and over the center of the bar (y = 9 m). The bar is located at $11 < x < 12.4$ m.

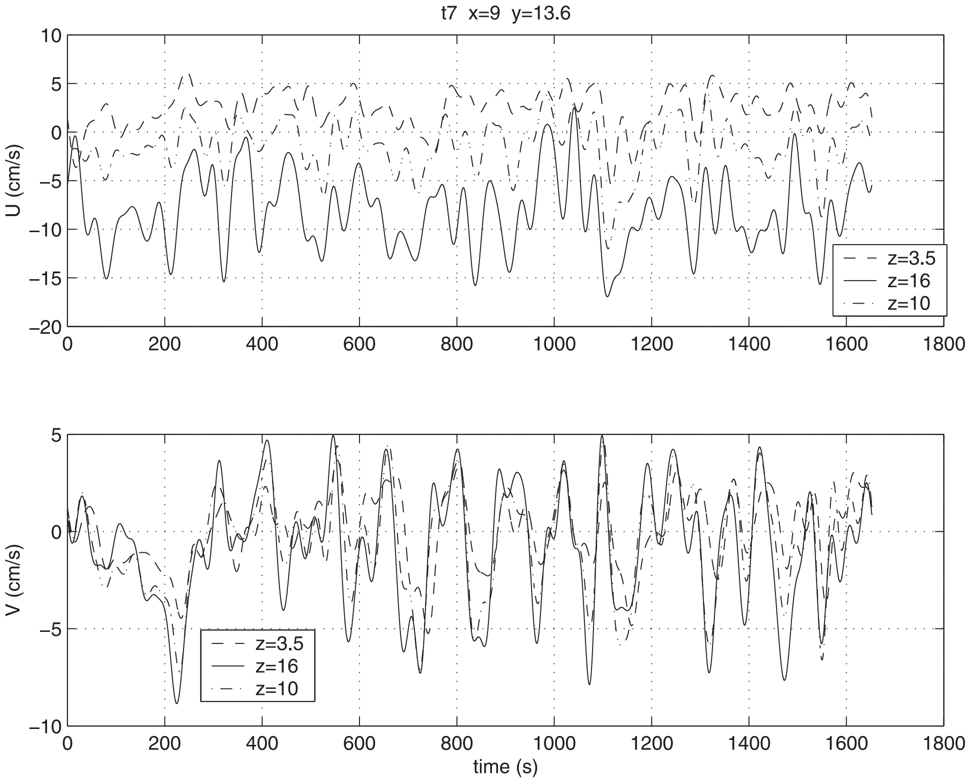

Figure 22. Low-pass filtered velocity time series at three depths 2 m offshore the channel (T7, x = 9.0 m). The top shows cross-shore velocities (U), and the bottom shows longshore velocities (V). The value of z is 0 at the bottom and is positive upward, measured in centimeters.

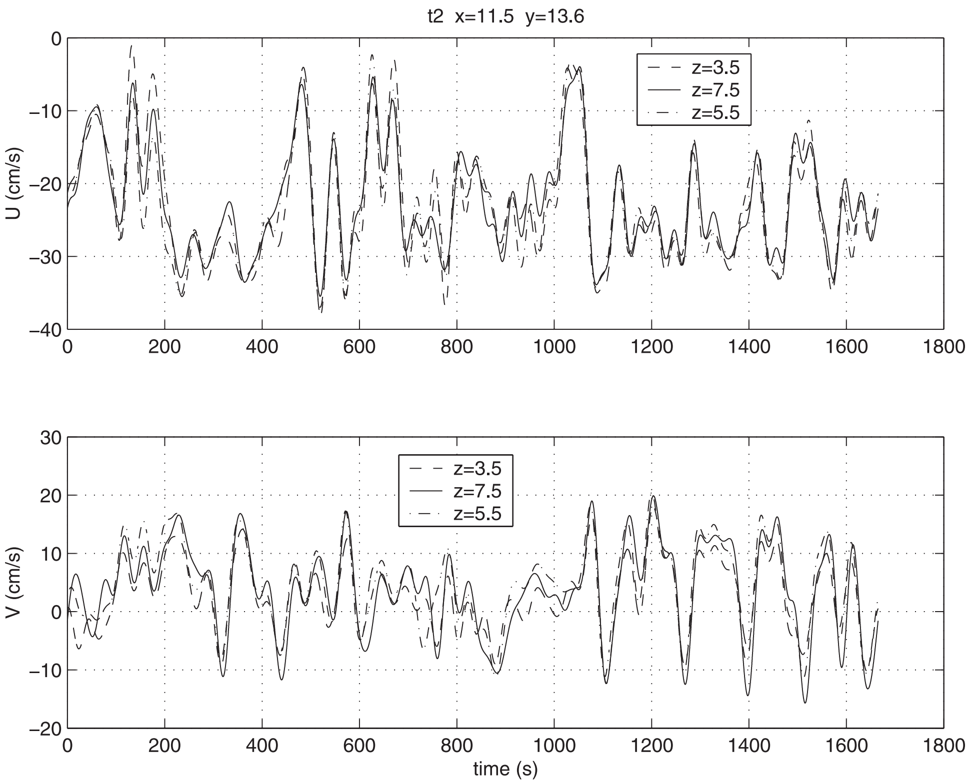

Figure 23. Low-pass filtered velocity time series at three depths inside the channel (T2, x = 11.5 m). The top shows cross-shore velocities (U), and the bottom shows longshore velocities (V). The value of z is 0 at the bottom and is positive upward, measured in centimeters.

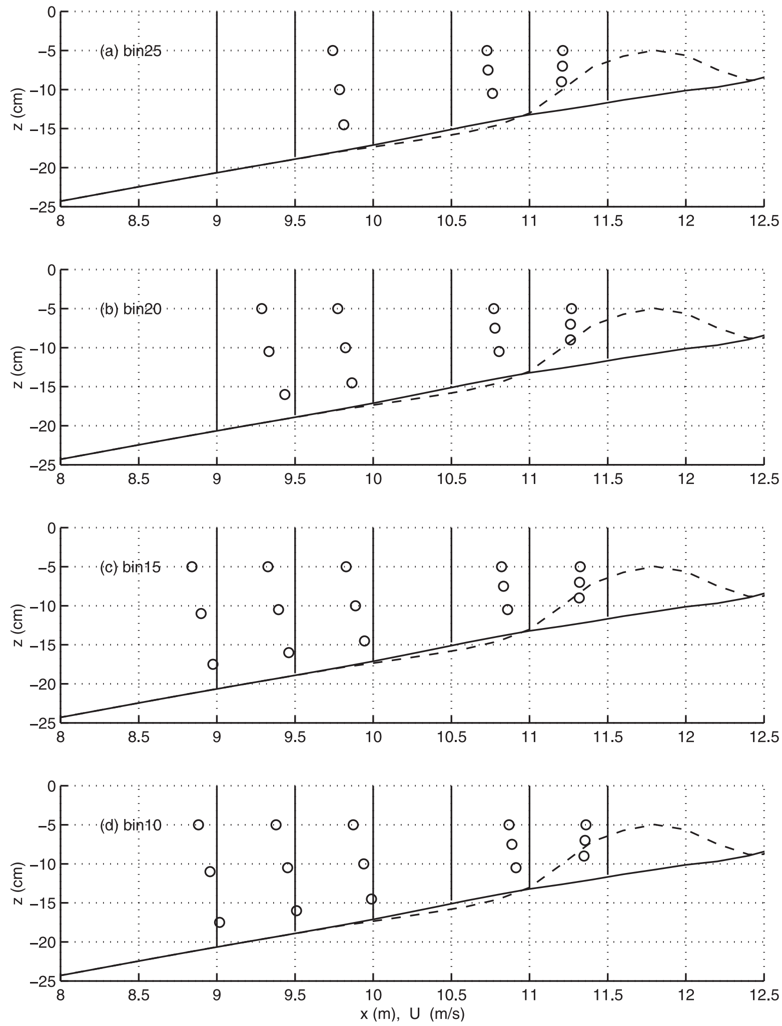

Figure 24. Bin-averaged rip current profiles from test T for (a) bin 25, (b) bin 20, (c) bin 15, and (d) bin 10. The vertical lines are the reference lines for each location.

[58] Figure 23 shows the similar low-pass filtered time series at three depths for the current inside the channel. Here the rip is much stronger inside the channel compared with the rip for the smaller waves in Figure 8. The current exceeds 35 cm/s, whereas for the previous tests the maximum current is only 25 cm/s. The current inside the channel has weak depth variations for both the small- and large-wave conditions.

[59] As with the other two tests, the current profiles are sorted into bins on the basis of the velocity from the gage closest to the surface following the method defined in section 3.1. The resulting profiles for each bin are shown in Figure 24. The profiles from x = 10.5 are not included because of problems with the synchronization of the gages at that location.

[60] In this case the bins contain more profiles because of the larger velocities associated with the bigger waves. However, the profiles in bin 10 are similar to the profiles for the smaller wave conditions in Figure 11. These profiles have strong depth variations in the offshore region ($x \leq 10$ m) with larger velocities close to the surface and weaker or shoreward velocities near the bottom. At x = 10 m the profile in bin 25 shows weaker depth variations than the profile in bin 10. The profile in bin 25 represents the maximum burst of rip flow, whereas the profile in bin 10 represents either the beginning or the ending of a rip burst. For all of the bins the profiles inside the channel are nearly depth-uniform.

[61] The larger waves carry more water over the bar, leading to greater offshore discharge in the rip currents. Because the depth is the same as for the smaller wave case, the larger discharge leads directly to larger velocities in the rip current. In addition, the larger flux in the rip causes the velocity at the bottom to be increased, leading to weaker vertical variation of the profiles.

4. Discussion

[62] As mentioned in section 1, field observations such as those by *Short* [1979], *Wright and Short* [1984], *Lippmann and Holman* [1990], and *Short and Brander* [1999] clearly suggest that rip currents are ubiquitous in the coastal environment and that they form an integral part of the coastal circulation systems responsible for the morphological development of littoral coasts. The rip currents constitute the principal relief current for the shoreward flow responsible for shoreward migration of longshore bars during accretion, and they are probably a leading mechanism for carrying sediments during storm erosion *Short* [1979]. It is therefore of interest to discuss the potential impact the measurements presented here could have on those processes.

[63] Because of the sporadic nature of the rips, the time-averaged mean velocities suggest that the rip does not extend far

outside the region of wave breaking. This would indicate that any sediment carried by the rip is only transported just outside the breakers. However, in reality the instantaneous velocities indicate that the rip does extend much farther offshore than the long time-averaged results suggest, and therefore the sediments would be carried much farther offshore.

[64] However, the sediment motions are primarily affected by the velocities closest to the bottom. Therefore the vertical variations of the rip current found in the experiments are also expected to have a profound impact on sediment transport that can be expected due to the rip current.

[65] In the rip channels where the velocity is almost depth-uniform, the rip currents clearly will have a tremendous transporting capacity. As the rip flows seaward, however, the weakening of, particularly, the velocities near the bottom will reduce the transport capacity of the rip. One can speculate that this eventually might lead to a redirectioning of the rip channel with profound impact on the flow patterns as a consequence. Predictions of sediment transport based on 2-D flow patterns would incorrectly predict scour throughout the whole offshore extent of the rip. Also, attempts to measure rip currents in the field must account for the vertical variation by taking the measurements outside the breaking region over the entire vertical.

[66] However, these speculations require much more extensive and detailed studies for final confirmation. The bin averaging and maximum averaging provide good spatial descriptions of the profiles. This facilitates comparisons with numerical models. Successful comparisons between the SHORECIRC model and data have been demonstrated by *Haas and Svendsen* [2000] and *Haas et al.* [2000]. The numerical model is also used to determine the reasons for the rip becoming a surface current. It is found through use of the numerical model that the vertical rip current profiles inside the channel are governed by the local forcing terms such as the pressure and the radiation stress gradients. However, offshore of the channel the nonlocal forcing terms, such as the convective accelerations, are responsible for the depth variations of the rip currents. It is extremely difficult to experimentally obtain enough instantaneous profiles to calculate the convective accelerations necessary to verify this mechanism. Therefore only enough measurements were taken to facilitate comparisons with the SHORECIRC model, and the determination of the mechanisms for the rip becoming a surface current are beyond the scope of this paper.

5. Conclusions

[67] Considered in combination with the *Haller and Dalrymple* [1999] experiments, the measurements described here represent the most comprehensive set of data of the 3-D circulation pattern for the most commonly occurring type of rip currents on sandy beaches. The experiments presented in this paper are primarily conducted to show the depth structure of rip currents. In brief, the experiments show that inside the channel where the waves are breaking, the rip currents are nearly depth-uniform. Offshore of the channel, however, we find that the rip current has strong depth variations, with strong seaward velocities in the upper half of the water column and weak seaward or landward velocities near the bottom.

[68] The depth variations are shown to be sensitive to the total volume flux in the rip. It turns out that the larger rip bursts containing more volume flux have less depth variation than smaller rip bursts at the same location. In the final test series it is found that the larger waves carry more water over the bar, leading to greater offshore discharge in the rip currents. Because the depth is the same as for the smaller wave case, the larger discharge leads directly to larger velocities in the rip current. In addition, the larger flux in the rip causes the velocity at the bottom to increase, leading to weaker vertical variation of the profiles.

[69] In addition to the depth variation the measurements indicate that the rip currents are unstable. At a given location the rip current appears sporadically and less frequently farther outside of the surf zone. The rip current is meandering from side to side within and offshore of the channel. There are even times when the rip moves out of the channel and over the bar or even vanishes all together. Repetition of the experiments with measurements at identical locations demonstrates the variability in the temporal development of the experiment. Because of the sporadic nature of the rip currents in time records of the velocities (especially offshore of the channel), long time averages of the velocities are not representative of the true velocities within the rip current. For this reason, bin-averaging and maximum-averaging techniques are used to demonstrate the cross-shore depth variations of the rip currents.

[70] **Acknowledgments.** This work was sponsored by Sea Grant under award NA96RG0029 and by ONR (contract N0014-99-1-1051). Merrick Haller is gratefully acknowledged for providing his rip current laboratory data and for providing guidance for our laboratory experiments.

References

Bakker, W., and T. van Doorn, Near-bottom velocities in waves with a current, in *Proceedings of the 16th Coastal Engineering Conference*, vol. 2, pp. 1394–1413, Am. Soc. of Civ. Eng., Reston, Va., 1978.

Brander, R. W., Measurements of flow velocity and sediment transport in a rip current, in *Proceedings of the 27th Coastal Engineering Conference*, pp. 3395–3408, Am. Soc. of Civ. Eng., Reston, Va., 2000.

Dalrymple, R. A., Rip currents and their causes, in *Proceedings of the 14th Coastal Engineering Conference*, pp. 1414-1427, Am. Soc. of Civ. Eng., Reston, Va., 1978.

Dingemans, M., J. A. T. M. van Kester, A. Radder, and R. Uittenbogaard, The effect of the CL-vortex force in 3D wave-current interaction, in *Proceedings of the 25th Coastal Engineering Conference*, vol. 4, pp. 4821–4832, Am. Soc. of Civ. Eng., Reston, Va., 1996.

Drønen, N., H. Karunarathna, J. Fredse, B. M. Sumer, and R. Deigaard, The circulation over a longshore bar with rip channels, in *Coastal Dynamics '97*, pp. 576–587, Am. Soc. of Civ. Eng., Reston, Va., 1999.

Haas, K. A., and I. A. Svendsen, Three-dimensional modeling of rip current systems, *Res. Rep. CACR-00-06*, Cent. for Appl. Coastal Res., Univ. of Del., Newark, 2000.

Haas, K. A., I. A. Svendsen, and M. Haller, Numerical modeling of nearshore circulation on a barred beach with rip channels, in *Proceedings of the 26th Coastal Engineering Conference*, vol. 1, pp. 801–814, Am. Soc. of Civ. Eng., Reston, Va., 1998.

Haas, K. A., I. A. Svendsen, and Q. Zhao, 3D modeling of rip currents, in *Proceedings of the 27th Coastal Engineering Conference*, vol. 2, pp. 1113–1126, Am. Soc. of Civ. Eng., Reston, Va., 2000.

Haller, M., and R. A. Dalrymple, Rip current dynamics and nearshore circulation, *Res. Rep. CACR-99-05*, Cent. for Appl. Coastal Res., Univ. of Del., Newark, Del., 1999.

Haller, M., R. Dalrymple, and I. A. Svendsen, Rip channels and nearshore circulation: Experiments, in *Proceedings Coastal Dynamics*, pp. 594–603, 1997a.

Haller, M., R. Dalrymple, and I. A. Svendsen, Experimental modeling of a rip current system, in *Proceedings of the 3rd International Symposium on Ocean Wave Measurement and Analysis*, pp. 750–764, Am. Soc. of Civ. Eng., Reston, Va., 1997b.

Haller, M. C., R. A. Dalrymple, and I. A. Svendsen, Experiments on rip currents and nearshore circulation: Data report, *Tech. Rep. CACR-00-04*, Cent. for Appl. Coastal Res., Univ. of Del., Newark, Del., 2000.

Kemp, P., and R. R. Simons, The interaction between waves and a turbulent current: Waves propagating with the current, *J. Fluid Mech.*, *116*, 227–250, 1982.

Kemp, P., and R. R. Simons, The interaction between waves and a turbulent current: Waves propagating against the current, *J. Fluid Mech.*, *130*, 73–89, 1983.

Klopman, G., Vertical structure of the flow due to waves and currents, *Tech. Prog. Rep. H840.30, Part II*, Delft Hydraul., Delft, 1994.

Lippmann, T. C., and R. A. Holman, The spatial and temporal variability of sand bar morphology, *J. Geophys. Res.*, *95*, 11,575–11,590, 1990.

Nielsen, P., and Z.-J. You, Eulerian mean velocities under non-breaking waves on horizontal bottoms, in *Proceedings of the 25th Coastal Engineering Conference*, vol. 4, pp. 4066–4078, Am. Soc. of Civ. Eng., Reston, Va., 1996.

Noda, E. K., Wave-induced nearshore circulation, *J. Geophys. Res.*, *79*, 4097–4106, 1974.

Sasaki, M., Velocity profiles in nearshore circulation current, *Coastal Eng. Jpn.*, *28*, 125–136, 1985.

Shepard, F. P., and D. L. Inman, Nearshore water circulation related to bottom topography and wave refraction, *Eos Trans. AGU*, *31*, 196–212, 1950.

Short, A. D., Three dimensional beach-stage model, *J. Geol.*, *87*, 553–571, 1979.

Short, A. D., and R. W. Brander, Regional variations in rip density, *J. Coastal Res.*, *15*, 813–822, 1999.

Sonu, C. J., Field observations of nearshore circulation and meandering currents, *J. Geophys. Res.*, *77*, 3232–3247, 1972.

Sørensen, O. R., H. A. Schäffer, P. A. Madsen, and R. Deigaard, Wave breaking and induced nearshore circulations, in *Proceedings of the 24th Coastal Engineering Conference*, pp. 2583–2594, Am. Soc. of Civ. Eng., Reston, Va., 1994.

Svendsen, I. A., K. A. Haas, and Q. Zhao, Analysis of rip current systems, in *Proceedings of the 27th Coastal Engineering Conference*, vol. 2, pp. 1127–1140, Am. Soc. of Civ. Eng., Reston, Va., 2000.

Tanaka, H., and A. Wada, Reproduction of nearshore currents by a mathematical model, *Coastal Eng. Jpn.*, *27*, 151–163, 1984.

Wind, H. G., and C. B. Vreugdenhil, Rip-current generation near structures, *J. Fluid Mech.*, *171*, 459–476, 1986.

Wright, L., and A. D. Short, Morphydynamic variability of surf zones and beaches: A synthesis, *Mar. Geol.*, *56*, 93–118, 1984.

K. A. Haas and I. A. Svendsen, Center for Applied Coastal Research, Ocean Engineering Lab, University of Delaware, Newark, DE 19716, USA. (haas@coastal.udel.edu; ias@coastal.udel.edu)